New evidence for the saturation of the Froissart bound

M. M. Block

Department of Physics and Astronomy, Northwestern University, Evanston, Illinois 60208, USA

F. Halzen

Department of Physics, University of Wisconsin, Madison, Wisconsin 53706, USA

(Received 3 June 2005; published 16 August 2005; publisher error corrected 17 August 2005)

Fits to high energy data alone cannot cleanly discriminate between asymptotic $\ln s$ and $\ln^2 s$ behavior of total hadronic cross sections. We demonstrate that this is no longer true when we require that these amplitudes *also* describe, on average, low energy data dominated by resonances. We simultaneously fit real analytic amplitudes to high energy measurements of: (i) the π^+p and π^-p total cross sections and ρ-values (ratio of the real to the imaginary portion of the forward scattering amplitude), for $\sqrt{s} \geq 6$ GeV, while requiring that the asymptotic fits smoothly join the σ_{π^+p} and σ_{π^-p} total cross sections at $\sqrt{s} = 2.6$ GeV—*both* in magnitude and slope , and (ii) separately simultaneously fit the $\bar{p}p$ and pp total cross sections and ρ-values for $\sqrt{s} \geq 6$ GeV, while requiring that their asymptotic fits smoothly join the the $\sigma_{\bar{p}p}$ and σ_{pp} total cross sections at $\sqrt{s} = 4.0$ GeV—again *both* in magnitude and slope. In both cases, we have used all of the extensive data of the Particle Data Group [K. Hagiwara *et al.* (Particle Data Group), Phys. Rev. D 66, 010001 (2002).]. However, we then subject these data to a screening process, the Sieve algorithm [M. M. Block, physics/0506010.], in order to eliminate outliers that can skew a χ^2 fit. With the Sieve algorithm, a robust fit using a Lorentzian distribution is first made to all of the data to sieve out abnormally high $\Delta\chi^2_i$, the individual ith point's contribution to the total χ^2. The χ^2 fits are then made to the sieved data. Both the πp and nucleon-nucleon systems strongly favor a high energy $\ln^2 s$ fit of the form: $\sigma^\pm = c_0 + c_1 \ln(\frac{\nu}{m}) + c_2 \ln^2(\frac{\nu}{m}) + \beta_{\mathcal{P}'}(\frac{\nu}{m})^{\mu-1} \pm \delta(\frac{\nu}{m})^{\alpha-1}$, basically excluding a $\ln s$ fit of the form: $\sigma^\pm = c_0 + c_1 \ln(\frac{\nu}{m}) + \beta_{\mathcal{P}'}(\frac{\nu}{m})^{\mu-1} \pm \delta(\frac{\nu}{m})^{\alpha-1}$. The upper sign is for π^+p (pp) and the lower sign is for π^-p ($\bar{p}p$) scattering, where ν is the laboratory pion (proton) energy, and m is the pion (proton) mass.

DOI: 10.1103/PhysRevD.72.036006 PACS numbers: 11.80.−m

High energy cross sections for the scattering of hadrons should be bounded by $\sigma \sim \ln^2 s$, where s is the square of the cms energy. This fundamental result is derived from unitarity and analyticity by Froissart [1], who states: "At forward or backward angles, the modulus of the amplitude behaves at most like $s\ln^2 s$, as s goes to infinity. We can use the optical theorem to derive that the total cross sections behave at most like $\ln^2 s$, as s goes to infinity". In this context, saturating the Froissart bound refers to an energy dependence of the total cross section rising no more rapidly than $\ln^2 s$.

The question as to whether any of the present day high energy data for $\bar{p}p$, pp and π^+p, π^-p cross sections saturate the Froissart bound has not been settled; one can not unambiguously discriminate between asymptotic fits of $\ln s$ and $\ln^2 s$ using high energy data only [2,3]. We here point out that this ambiguity is resolved by requiring that the fits to the high energy data smoothly join the cross section and energy dependence obtained by averaging the resonances at low energy. Imposing this duality [4] condition, we show that only fits to the high energy data behaving as $\ln^2 s$ that smoothly join (in *both* magnitude and first derivative) to the low energy data at the "transition energy" (defined as the energy region just after the resonance regions end) can adequately describe the highest energy points. This technique has recently been successfully used by Block and Halzen[5] to show that the Froissart bound is saturated for the γp system.

We will use real analytic amplitudes to describe the data. Following Block and Cahn [6], we write the crossing-even real analytic amplitude for high energy scattering as [5,7]

$$f_+ = i\frac{\nu}{4\pi}\left\{A + \beta[\ln(s/s_0) - i\pi/2]^2 + cs^{\mu-1}e^{i\pi(1-\mu)/2} - i\frac{4\pi}{\nu}f_+(0)\right\}, \tag{1}$$

and the crossing-odd real analytic amplitude as

$$f_- = -Ds^{\alpha-1}e^{i\pi(1-\alpha)/2}. \tag{2}$$

Here $\alpha < 1$ parametrizes the Regge behavior of the crossing-odd amplitude which vanishes at high energies and A, α, β, c, D, s_0 and μ are real constants. The variable s is the square of the center of mass system (cms) energy and ν is the laboratory energy. The additional real constant $f_+(0)$ is the subtraction constant at $\nu = 0$ needed to be introduced in a singly-subtracted dispersion relation [6,8]. Using the optical theorem, we obtain the total cross section

$$\sigma^\pm = A + \beta\left[\ln^2 s/s_0 - \frac{\pi^2}{4}\right] + c\sin(\pi\mu/2)s^{\mu-1} \pm D\cos(\pi\alpha/2)s^{\alpha-1} \tag{3}$$

with ρ, the ratio of the real to the imaginary part of the forward scattering amplitude, given by

$$\rho^{\pm} = \frac{1}{\sigma_{\rm tot}}\left\{\beta\pi \ln s/s_0 - c\cos(\pi\mu/2)s^{\mu-1} + \frac{4\pi}{\nu}f_+(0) \pm D\sin(\pi\alpha/2)s^{\alpha-1}\right\}, \tag{4}$$

where the upper sign is for π^+p (pp) and the lower sign is for π^-p ($\bar{p}p$) scattering, and the even amplitude applies to the spin-averaged γp scattering [5].

We now introduce the definitions $A = c_0 + \frac{\pi^2}{4}c_2 - \frac{c_1^2}{4c_2}$, $s_0 = 2m^2e^{-c_1/(2c_2)}$, $\beta = c_2$, $c = \frac{(2m^2)^{1-\mu}}{\sin(\pi\mu/2)}\beta_{\mathcal{P}'}$ and $D = \frac{(2m^2)^{1-\alpha}}{\cos(\pi\alpha/2)}\delta$. In the high energy limit, where $s \to 2m\nu$, Eq. (3) and (4), along with their cross section derivatives $\frac{d\sigma^\pm}{d(\nu/m)}$, can be written as

$$\sigma^{\pm} = c_0 + c_1\ln\left(\frac{\nu}{m}\right) + c_2\ln^2\left(\frac{\nu}{m}\right) + \beta_{\mathcal{P}'}\left(\frac{\nu}{m}\right)^{\mu-1} \pm \delta\left(\frac{\nu}{m}\right)^{\alpha-1}, \tag{5}$$

$$\rho^{\pm} = \frac{1}{\sigma^{\pm}}\left\{\frac{\pi}{2}c_1 + c_2\pi\ln\left(\frac{\nu}{m}\right) - \beta_{\mathcal{P}'}\cot\left(\frac{\pi\mu}{2}\right)\left(\frac{\nu}{m}\right)^{\mu-1} + \frac{4\pi}{\nu}f_+(0) \pm \delta\tan\left(\frac{\pi\alpha}{2}\right)\left(\frac{\nu}{m}\right)^{\alpha-1}\right\}, \tag{6}$$

$$\frac{d\sigma^{\pm}}{d((\nu/m)} = c_1\left\{\frac{1}{(\nu/m)}\right\} + c_2\left\{\frac{2\ln(\nu/m)}{(\nu/m)}\right\} + \beta_{\mathcal{P}'}\{(\mu-1) \times (\nu/m)^{\mu-2}\} \pm \delta\{(\alpha-1)(\nu/m)^{\alpha-2}\}, \tag{7}$$

where the upper sign is for π^+p (pp) and the lower sign is for π^-p ($\bar{p}p$) scattering. The exponents μ and α are real. This transformation linearizes Eq. (5) in the real coefficients $c_0, c_1, c_2, \beta_{\mathcal{P}'}$ and δ, convenient for a χ^2 fit to the experimental total cross sections and ρ-values. Throughout we will use units of ν and m in GeV and cross section in mb, where m is the projectile mass.

Let σ^+ be the total cross section for π^+p (pp) scattering and σ^- the total cross section for π^-p ($\bar{p}p$) scattering. It is convenient to define, at the transition energy ν_0,

$$\sigma_{\rm av} = \frac{\sigma^+(\nu_0/m) + \sigma^-(\nu_0/m)}{2} = c_0 + c_1\ln(\nu_0/m) + c_2\ln^2(\nu_0/m) + \beta_{\mathcal{P}'}(\nu_0/m)^{\mu-1}, \tag{8}$$

$$\Delta\sigma = \frac{\sigma^+(\nu_0/m) - \sigma^-(\nu_0/m)}{2} = \delta(\nu_0/m)^{\alpha-1}, \tag{9}$$

$$m_{\rm av} = \frac{1}{2}\left(\frac{d\sigma^+}{d(\nu/m)} + \frac{d\sigma^-}{d(\nu/m)}\right)_{\nu=\nu_0} = c_1\left\{\frac{1}{(\nu_0/m)}\right\} + c_2\left\{\frac{2\ln(\nu_0/m)}{(\nu_0/m)}\right\} + \beta_{\mathcal{P}'}\{(\mu-1)(\nu_0/m)^{\mu-2}\}, \tag{10}$$

$$\Delta m = \frac{1}{2}\left(\frac{d\sigma^+}{d(\nu/m)} - \frac{d\sigma^-}{d(\nu/m)}\right)_{\nu=\nu_0} = \delta\{(\alpha-1)(\nu_0/m)^{\alpha-2}\}. \tag{11}$$

Using the definitions of $\sigma_{\rm av}$, $\Delta\sigma$, $m_{\rm av}$ and Δm, we now write the four constraint equations

$$\beta_{\mathcal{P}'} = \frac{(\nu_0/m)^{2-\mu}}{\mu-1}\left[m_{\rm av} - c_1\left\{\frac{1}{(\nu_0/m)}\right\} - c_2\left\{\frac{2\ln(\nu_0/m)}{(\nu_0/m)}\right\}\right], \tag{12}$$

$$c_0 = \sigma_{\rm av} - c_1\ln(\nu_0/m) - c_2\ln^2(\nu_0/m) - \beta_{\mathcal{P}'}(\nu_0/m)^{\mu-1}, \tag{13}$$

$$\alpha = 1 + \frac{\Delta m}{\Delta\sigma}(\nu_0/m), \tag{14}$$

$$\delta = \Delta\sigma(\nu_0/m)^{1-\alpha}, \tag{15}$$

that utilize the two slopes and the two intercepts at the transition energy ν_0, where we join on to the asymptotic fit. We pick ν_0 as the (very low) energy just after which resonance behavior finishes. We use $\mu = 0.5$ throughout, which is appropriate for a Regge-descending trajectory. In the above, $m = m_p$ is the proton mass for the $\bar{p}p$ and pp systems, while $m = m_\pi$ is the pion mass for the π^-p and π^+p systems.

Our strategy is to use the rich amount of low energy data to constrain our high energy fit. At the transition energy ν_0, the cross sections $\sigma^+(\nu_0/m)$ and $\sigma^-(\nu_0/m)$, along with the slopes $(\frac{d\sigma^+}{d((\nu/m)})_{\nu=\nu_0}$ and $(\frac{d\sigma^-}{d((\nu/m)})_{\nu=\nu_0}$, are used to constrain the asymptotic high energy fit so that it matches the low energy data at the transition energy ν_0. We pick ν_0 much below the energy at which we start our high energy fit, but at an energy safely above the resonance regions. Very local fits are made to the region about the energy ν_0 in order to evaluate the two cross sections and their two derivatives at ν_0 that are needed in the above constraint equations. We next impose the 4 constraint equations, Eqs. (12)–(15), which we use in our χ^2 fit to Eqs. (5) and (6). For safety, we start the data fitting at an energy $\nu_{\rm min}$ appreciably higher than the transition energy. The transition energies, with appropriate cross sections and slopes, are summarized in Table I, along with the minimum energies used in the asymptotic fits.

TABLE I. The transition energy parameters used for fitting $\pi^+ p$, $\pi^- p$, pp and $\bar{p}p$ scattering.

Transition Energy Parameters	$\pi^+ p$ and $\pi^- p$ Scattering	pp and $\bar{p}p$ Scattering
ν_0, lab transition energy (GeV)	3.12	7.59
$\rightarrow \sqrt{s}0$, cms transition energy (GeV)	2.6	4
$\sigma^+(\nu_0)$ (mb)	28.91	40.18
$\sigma^-(\nu_0)$ (mb)	32.04	56.99
$(\frac{d\sigma^+}{d(\nu/m)})_{\nu=\nu_0}$ (mb)	-0.2305	-0.2262
$(\frac{d\sigma^-}{d(\nu/m)})_{\nu=\nu_0}$ (mb)	-1.446	-0.2740
Minimum fitting energy		
$\nu_{\rm min}$, lab minimum energy (GeV)	18.71	18.25
$\rightarrow \sqrt{s}\,\mathrm{min}$, cms minimum energy (GeV)	6.0	6.0
m is the pion (proton) mass and ν is the laboratory pion (proton) energy		

We stress that the odd amplitude parameters α and δ and hence the odd amplitude itself is *completely determined* by the experimental values Δm and $\Delta\sigma$ at the transition energy ν_0. Thus, at *all* energies, the *differences* of the cross sections $\sigma^- - \sigma^+$ (from the optical theorem, the differences in the imaginary portion of the scattering amplitude) and the *differences* of the real portion of the scattering amplitude are completely fixed *before* we make our fit. Further, for a $\ln^2 s$ ($\ln s$) fit, the even amplitude parameters c_0 and $\beta'_{\mathcal{P}}$ are determined by c_1 and c_2 (c_1 only) along with the experimental values of $\sigma_{\rm av}$ and $m_{\rm av}$ at the transition energy ν_0. In particular, for a $\ln^2 s$ ($\ln s$) fit, we only fit the 3 (2) parameters c_1, c_2, and $f(0)$ (c_1 and $f_+(0)$). Since the subtraction constant $f_+(0)$ only enters into the ρ-value determinations, only the 2 parameters c_1 and c_2 of the original 7 are required for a $\ln^2 s$ fit to the cross sections $\sigma^\pm$, which gives us exceedingly little freedom in this fit—it is indeed very tightly constrained, with not much latitude for adjustment. The cross sections $\sigma^\pm$ for the $\ln s$ fit are even more tightly constrained, with only one adjustable parameter, c_1.

We now outline the adaptive Sieve algorithm [9] that minimizes the effect that "outliers"—points with abnormally high contributions to χ^2—have on a fit when they contaminate a data sample that is otherwise Gaussianly distributed. Our fitting procedure consists of several steps:

(1) Make a robust fit of *all* of the data (presumed outliers and all) by minimizing Λ_0^2, the Lorentzian squared with respect to $\boldsymbol{\alpha}$, where

$$\Lambda_0^2(\boldsymbol{\alpha};\boldsymbol{x}) \equiv \sum_{i=1}^{N} \ln\{1 + 0.179\Delta\chi_i^2(x_i;\boldsymbol{\alpha})\}, \qquad (16)$$

with $\boldsymbol{\alpha} = \{\alpha_1, \ldots, \alpha_M\}$ being the M-dimensional parameter space of the fit. $\boldsymbol{x} = \{x_1, \ldots, x_N\}$ represents the abscissa of the N experimental measurements $\boldsymbol{y} = \{y_1, \ldots, y_N\}$ that are being fit and $\Delta\chi_i^2(x_i;\boldsymbol{\alpha}) \equiv (\frac{y_i - y(x_i;\boldsymbol{\alpha})}{\sigma_i})^2$ is the individual χ^2 contribution of the $i^{\rm th}$ point, where $y(x_i;\boldsymbol{\alpha})$ is the theoretical value at x_i and σ_i is the experimental error. It is shown in Ref. [9] that for Gaussianly distributed data, minimizing Λ_0^2 gives, on average, the same total $\chi^2_{\rm min} \equiv \sum_{i=1}^{N} \Delta\chi_i^2(x_i;\boldsymbol{\alpha})$ from Eq. (16) as that found in a conventional χ^2 fit, as well as rms widths (errors) for the parameters that are almost the same as those found in a χ^2 fit.

A quantitative measure of whether point i is an outlier, i.e., whether it is "far away" from the true signal, is the magnitude of its $\Delta\chi_i^2(x_i;\boldsymbol{\alpha}) = (\frac{y_i - y(x_i;\boldsymbol{\alpha})}{\sigma_i})^2$. The reason for minimizing the Lorentzian squared is that this procedure gives the outliers much less weight w in the fit ($w \propto 1/\sqrt{\Delta\chi_i^2(x_i;\boldsymbol{\alpha})}$), for large $\Delta\chi_i^2(x_i;\boldsymbol{\alpha})$ than does a χ^2 fit ($w \propto \sqrt{\Delta\chi_i^2(x_i;\boldsymbol{\alpha})}$), thus making the fitted parameters insensitive to outliers and hence robust. For details, see Ref. [9].

If $\chi^2_{\rm min}$ is satisfactory, make a conventional χ^2 fit to get the errors and you are finished. If $\chi^2_{\rm min}$ is not satisfactory, proceed to step 2.

(2) Using the above robust Λ_0^2 fit as the initial estimator for the theoretical curve, evaluate $\Delta\chi_i^2(x_i;\boldsymbol{\alpha})$, for each of the N experimental points.

(3) A largest cut, $\Delta\chi_i^2(x_i;\boldsymbol{\alpha})_{\rm max}$, must now be selected. We start the process with $\Delta\chi_i^2(x_i;\boldsymbol{\alpha})_{\rm max} = 9$. If any of the points have $\Delta\chi_i^2(x_i;\boldsymbol{\alpha}) > \Delta\chi_i^2(x_i;\boldsymbol{\alpha})_{\rm max}$, reject them—they fell through the "Sieve". The choice of $\Delta\chi_i^2(x_i;\boldsymbol{\alpha})_{\rm max}$ is an attempt to pick the largest Sieve size (largest $\Delta\chi_i^2(x_i;\boldsymbol{\alpha})_{\rm max}$) that rejects all of the outliers, while minimizing the number of signal points rejected.

(4) Next, make a conventional χ^2 fit to the sifted set—these data points are the ones that have been retained in the Sieve. This fit is used to estimate $\chi^2_{\rm min}$. Since the data set has been truncated by eliminating the points with $\Delta\chi_i^2(x_i;\boldsymbol{\alpha}) > \Delta\chi_i^2(x_i;\boldsymbol{\alpha})_{\rm max}$, we must slightly renormalize the $\chi^2_{\rm min}$ found to take this into account, by the factor $\mathcal{R}$. For $\Delta\chi^2_{i\,\rm max} = 9, 6,$ and 4, the factor $\mathcal{R}$ is given by 1.027, 1.140 and 1.291, whereas the fraction of the points that should survive this χ^2 cut—for a Gaussian distribution—is

0.9973, 0.9857 and 0.9545, respectively. A plot of $\mathcal{R}^{-1}$ as a function of $\Delta\chi^2_{i\,\max}$ is given in Fig. 1, which is taken from Ref. [9].

If the renormalized $\chi^2_{\min}$, i.e., $\mathcal{R} \times \chi^2_{\min}$ is acceptable—in the *conventional* sense, using the ordinary χ^2 distribution probability function—we consider the fit of the data to the model to be satisfactory and proceed to the next step. If the renormalized $\chi^2_{\min}$ is not acceptable and $\Delta\chi^2_i(x_i;\boldsymbol{\alpha})_{\max}$ is not too small, we pick a smaller $\Delta\chi^2_i(x_i;\boldsymbol{\alpha})_{\max}$ and go back to step 3. The smallest value of $\Delta\chi^2_i(x_i;\boldsymbol{\alpha})_{\max}$ that we used is $\Delta\chi^2_i(x_i;\boldsymbol{\alpha})_{\max} = 4$.

(5) From the χ^2 fit that was made to the "sifted" data in the preceding step, evaluate the parameters $\boldsymbol{\alpha}$. Next, evaluate the $M \times M$ covariance (squared error) matrix of the parameter space which was found in the χ^2 fit. We find the new squared error matrix for the Λ^2 fit by multiplying the covariance matrix by the square of the factor r_{χ^2}. From Fig. 1, we find that $r_{\chi^2} \sim 1.02, 1.05$ and 1.11 for $\Delta\chi^2_i(x_i;\boldsymbol{\alpha})_{\max} = 9$, 6 and 4, respectively. The values of $r_{\chi^2} > 1$ reflect the fact that a χ^2 fit to the *truncated* Gaussian distribution that we obtain—after first making a robust fit—has a rms (root mean square) width which is somewhat greater than the rms width of the χ^2 fit to the same untruncated distribution [9].

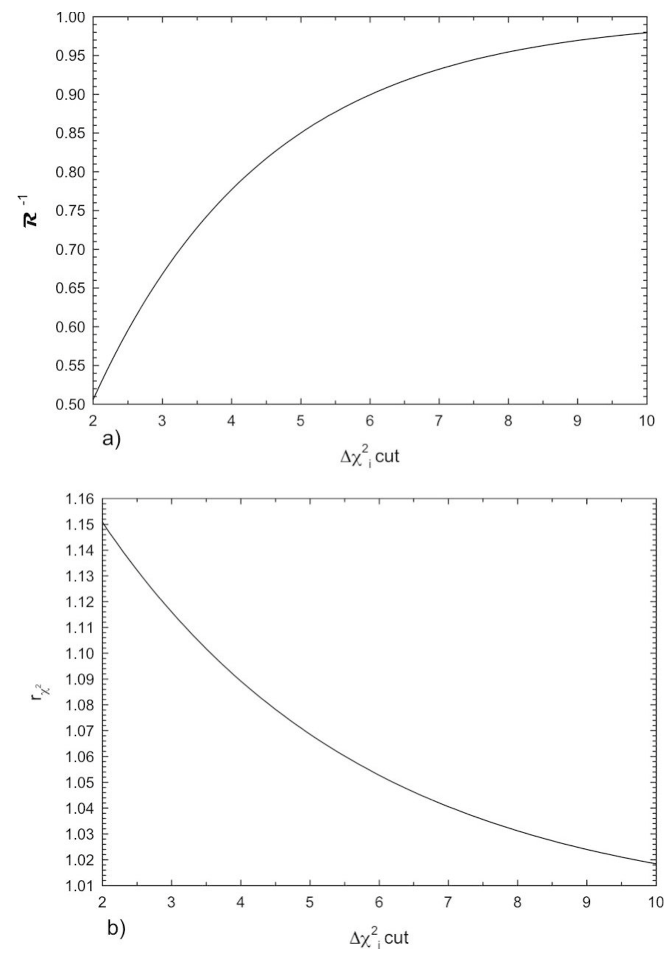

FIG. 1. (a) A plot of $\mathcal{R}^{-1}$, the reciprocal of the factor that multiplies $\chi^2_{\min}/\nu$ found in the χ^2 fit to the sifted data set *vs.* $\Delta\chi^2_i$ cut, *i.e.,* $\Delta\chi^2_{i\,\max}$. (b) A plot of r_{χ^2}, the factor whose square multiplies the covariant matrix found in the χ^2 fit to the sifted data set *vs.* $\Delta\chi^2_i$ cut, i.e., $\Delta\chi^2_{i\,\max}$. These figures are taken from Ref. [9].

The application of a χ^2 fit to the *sifted set* gives stable estimates of the model parameters $\boldsymbol{\alpha}$, as well as a goodness-of-fit of the data to the model when $\chi^2_{\min}$ is renormalized for the effect of truncation due to the cut $\Delta\chi^2_i(x_i;\boldsymbol{\alpha})_{\max}$. One can now use conventional probabilities for χ^2 fits, *i.e.,* the probability that χ^2 is greater than $\mathcal{R} \times \chi^2_{\min}$, for the number of degrees of freedom ν. Model parameter errors are found by multiplying the covariance (squared error) matrix of the conventional χ^2 fit by the appropriate factor $(r_{\chi^2})^2$ for the cut $\Delta\chi^2_i(x_i;\boldsymbol{\alpha})_{\max}$.

Table II summarizes the results of our simultaneous fits to all of the available data from the Particle Data Group [10] for σ_{π^+p}, σ_{π^-p}, ρ_{π^+p} and ρ_{π^-p}, using the 4 constraint equations with a transition energy $\sqrt{s} = 2.6$ GeV and a minimum fitting energy of 6 GeV, after applying the Sieve algorithm [9]. Three $\Delta\chi^2_{i\,\max}$ cuts, 4, 6 and 9, were made for $\ln^2(\nu/m_\pi)$ fits. There was considerable improvement in the renormalized χ^2/d.f. going from $\Delta\chi^2_{i\,\max} = 9$ to $\Delta\chi^2_{i\,\max} = 6$. However, there was no improvement of the renormalized χ^2/d.f. going from $\Delta\chi^2_{i\,\max} = 6$ to $\Delta\chi^2_{i\,\max} = 4$—indeed, it increased from 1.294 to 1.364. Since the errors also become substantially larger for the $\Delta\chi^2_{i\,\max} = 4$ cut, we chose to use the values of the $\ln^2(\nu/m_\pi)$ fit with a $\Delta\chi^2_{i\,\max} = 6$ cut. This cut was therefore also used for the $\ln(\nu/m_\pi)$ fit. The probability of the fit for the data set using the $\Delta\chi^2_{i\,\max} = 6$ cut was $\sim$0.02, a somewhat low probability, albeit one that is often deemed acceptable in a fit with this many degrees of freedom (d.f. = 127). In contrast, the probability of the $\ln(\nu/m_\pi)$ fit using the $\Delta\chi^2_{i\,\max} = 6$ data set is $<< 10^{-16}$ and is clearly ruled out, as is graphically demonstrated in Fig. 2.

It should be noted that when using a $\ln^2(\nu/m_\pi)$ fit *before* imposing the Sieve algorithm, a value of $\chi^2/\text{d.f.} = 3.472$ for 152 degrees of freedom was found, compared to $\chi^2/\text{d.f.} = 1.294$ for 127 degrees of freedom when using the $\Delta\chi^2_{i\,\max} = 6$ cut. In essence, the Sieve algorithm eliminated 25 points with energies $\sqrt{s} \geq 6$ GeV (2 σ_{π^+p}, 19 σ_{π^-p}, 4 ρ_{π^+p}), while changing the total renormalized χ^2 from 527.8 to 164.3. These 25 points that were screened out had a χ^2 contribution of 363.5, an average value of 14.5. If the distribution had been Gaussian with no outliers, one would have expected about 2 points having $\Delta\chi^2_i > 6$, giving a total χ^2 contribution slightly larger than 12, compared to the observed value of 363.5. Thus, we see the effect of the Sieve algorithm in cleaning up the data sample by eliminating the outliers.

TABLE II. The fitted results for a 3-parameter χ^2 fit with $\sigma \sim \ln^2(\nu/m_\pi)$ and a 2-parameter fit with $\sigma \sim \ln(\nu/m_\pi)$ to the total cross sections and ρ-values for $\pi^+ p$ and $\pi^- p$ scattering. The renormalized $\chi^2/\nu_{\rm min}$, taking into account the effects of the $\Delta\chi^2_{i\,\rm max}$ cut, is given in the row labeled $\mathcal{R} \times \chi^2_{\rm min}/\nu$. The errors in the fitted parameters have been multiplied by the appropriate $r_{\chi 2}$. The pion mass is m_π and the laboratory pion energy is ν.

Parameters	$\sigma \sim \ln^2(\nu/m_\pi)$ $\Delta\chi^2_{i\,\rm max}$		$\sigma \sim \ln(\nu/m_\pi)$ $\Delta\chi^2_{i\,\rm max}$
	6	9	6
	Even Amplitude		
c_0 (mb)	20.11	20.32	12.75
c_1 (mb)	-0.921 ± 0.110	-0.981 ± 0.100	1.286 ± 0.0056
c_2 (mb)	0.1767 ± 0.0085	0.1815 ± 0.0077	—
$\beta_{\mathcal{P}'}$ (mb)	54.40	54.10	64.87
μ	0.5	0.5	0.5
$f(0)$ (mb GeV)	-2.33 ± 0.36	-2.31 ± 0.35	0.34 ± 0.36
	Odd Amplitude		
δ (mb)	-4.51	-4.51	-4.51
α	0.660	0.660	0.660
$\chi^2_{\rm min}$	148.1	204.4	941.8
$\mathcal{R} \times \chi^2_{\rm min}$	164.3	210.0	1044.9
ν (d.f).	127	135	128
$\mathcal{R} \times \chi^2_{\rm min}/\nu$	1.294	1.555	8.163

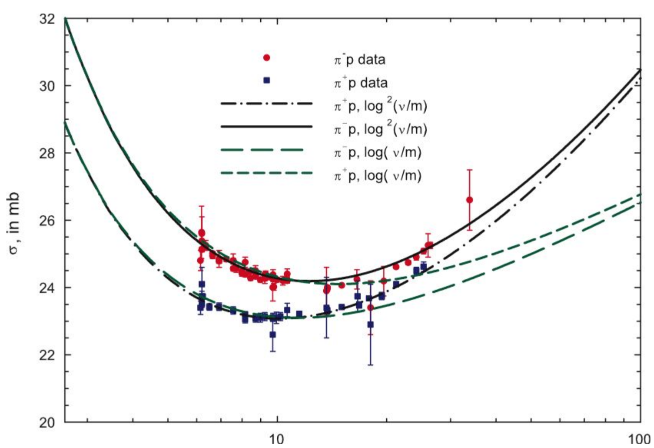

FIG. 2 (color online). The fitted total cross sections $\sigma_{\pi^+ p}$ and $\sigma_{\pi^- p}$ in mb, *vs.* $\sqrt{s}$, in GeV, using the 4 constraints of Eqs. (12)–(15). The circles are the sieved data for $\pi^- p$ scattering and the squares are the sieved data for $\pi^+ p$ scattering for $\sqrt{s} \geq 6$ GeV. The dash-dotted curve ($\pi^+ p$) and the solid curve ($\pi^- p$) are χ^2 fits (Table II, $\sigma \sim \ln^2(\nu/m_\pi)$, $\Delta\chi^2_{i\,\rm max} = 6$) of the high energy data of the form : $\sigma_{\pi^\pm p} = c_0 + c_1 \ln(\frac{\nu}{m}) + c_2 \ln^2(\frac{\nu}{m}) + \beta_{\mathcal{P}'}(\frac{\nu}{m})^{\mu-1} \pm \delta(\frac{\nu}{m})^{\alpha-1}$. The upper sign is for $\pi^+ p$ and the lower sign is for $\pi^- p$ scattering. The short dashed curve ($\pi^+ p$) and the long dashed curve ($\pi^- p$) are χ^2 fits (Table II, $\sigma \sim \ln(\nu/m_\pi)$, $\Delta\chi^2_{i\,\rm max} = 6$) of the high energy data of the form : $\sigma_{\pi^\pm p} = c_0 + c_1 \ln(\frac{\nu}{m}) + \beta_{\mathcal{P}'}(\frac{\nu}{m})^{\mu-1} \pm \delta(\frac{\nu}{m})^{\alpha-1}$. The upper sign is for $\pi^+ p$ and the lower sign is for $\pi^- p$ scattering. The laboratory energy of the pion is ν and m is the pion mass.

Next, we analyze the $\bar{p}p$ and pp systems. Table III summarizes the results of our simultaneous fits to the available accelerator data from the Particle Data Group [10] for σ_{pp}, $\sigma_{\bar{p}p}$, ρ_{pp} and $\rho_{\bar{p}p}$, using the 4 constraint equations with a transition energy $\sqrt{s} = 4$ GeV and a minimum fitting energy of 6 GeV, again using the Sieve algorithm. Two $\Delta\chi^2_{i\,\rm max}$ cuts, 6 and 9, were made for $\ln^2(\nu/m_p)$ fits. The probability of the fit for the cut $\Delta\chi^2_{i\,\rm max} = 6$ was ~ 0.2, a very satisfactory probability for this many degrees of freedom, and we chose this data set rather than the data set corresponding to the $\Delta\chi^2_{i\,\rm max} = 9$ cut. As seen in Table III, the fitted parameters are very insensitive to this choice. The same data set ($\Delta\chi^2_{i\,\rm max} = 6$ cut) was also used for the $\ln(\nu/m_p)$ fit. The probability of the $\ln(\nu/m_p)$ fit is $<< 10^{-16}$ and is clearly ruled out. This is illustrated graphically in Fig. 6 and 7.

We note that when using a $\ln^2(\nu/m_p)$ fit *before* imposing the Sieve algorithm, a value of $\chi^2/\text{d.f.} = 5.657$ for 209 degrees of freedom was found, compared to $\chi^2/\text{d.f.} = 1.095$ for 184 degrees of freedom when using the $\Delta\chi^2_{i\,\rm max} = 6$ cut. The Sieve algorithm eliminated 25 points with energies $\sqrt{s} \geq 6$ GeV (5 σ_{pp}, 5 $\sigma_{\bar{p}p}$, 15 ρ_{pp}), while changing the total renormalized χ^2 from 1182.3 to 201.4. These 25 points that were screened out had a χ^2 contribution of 980.9, an average value of 39.2. For a Gaussian distribution, about 3 points with $\Delta\chi^2_i > 6$ are expected, with a total χ^2 contribution of slightly more than 18 and *not* 980.9. Again, we see the effect of the Sieve algorithm in ridding the data sample of outliers.

TABLE III. The fitted results for a 3-parameter χ^2 fit with $\sigma \sim \ln^2(\nu/m_p)$ and a 2-parameter fit with $\sigma \sim \ln(\nu/m_p)$ to the total cross sections and ρ-values for pp and $\bar{p}p$ scattering. The renormalized $\chi^2/\nu_{\rm min}$, taking into account the effects of the $\Delta\chi^2_{i\,\rm max}$ cut, is given in the row labeled $\mathcal{R}\times\chi^2_{\rm min}/\nu$. The errors in the fitted parameters have been multiplied by the appropriate $r_{\chi 2}$. The proton mass is m_p and the laboratory nucleon energy is ν.

Parameters	$\sigma \sim \ln^2(\nu/m_p)$ $\Delta\chi^2_{i\,\rm max}$		$\sigma \sim \ln(\nu/m_p)$ $\Delta\chi^2_{i\,\rm max}$
	6	9	6
	Even Amplitude		
c_0 (mb)	37.32	37.25	28.26
c_1 (mb)	-1.440 ± 0.070	-1.416 ± 0.066	2.651 ± 0.0070
c_2 (mb)	0.2817 ± 0.0064	0.2792 ± 0.0059	—
$\beta_{\mathcal{P}'}$ (mb)	37.10	37.17	47.98
μ	0.5	0.5	0.5
$f(0)$ (mb GeV)	-0.075 ± 0.59	-0.069 ± 0.57	4.28 ± 0.59
	Odd Amplitude		
δ (mb)	-28.56	-28.56	-28.56
α	0.415	0.415	0.415
$\chi^2_{\rm min}$	181.6	216.6	2355.7
$\mathcal{R}\times\chi^2_{\rm min}$	201.5	222.5	2613.7
ν (d.f).	184	189	185
$\mathcal{R}\times\chi^2_{\rm min}/\nu$	1.095	1.178	14.13

Figure 2 shows the individual fitted cross sections (in mb) for π^+p and π^-p for $\ln^2(\nu/m_\pi)$ and $\ln(\nu/m_\pi)$, for the cut $\Delta\chi^2_{i\,\rm max} = 6$, from Table II plotted against the cms energy, $\sqrt{s}$, in GeV. The data shown are the sieved data with $\sqrt{s} \ge 6$ GeV. The $\ln^2(\nu/m_\pi)$ fits with $\Delta\chi^2_{i\,\rm max} = 6$ corresponding to the solid curve for π^-p and the dash-dotted curve for π^+p, are in excellent agreement with the cross section data. On the other hand, the $\ln(\nu/m_\pi)$ fits—the long dashed curve for π^-p and the short dashed curve for π^+p—although they fit in the low energy region almost identically to the $\ln^2(\nu/m_\pi)$ fits—are very bad fits which clearly underestimate *all* of the high energy cross sections, leading to huge $\chi^2_{\rm min}$, and hence are ruled out.

Figure 3 shows the individual fitted ρ-values for π^+p and π^-p for $\ln^2(\nu/m_\pi)$ and $\ln(\nu/m_\pi)$, for the cut $\Delta\chi^2_{i\,\rm max} = 6$, from Table II, *vs.* $\sqrt{s}$, the cms energy in GeV. The data shown are the sieved data with $\sqrt{s} \ge 6$ GeV. The $\ln^2(\nu/m_\pi)$ fits with $\Delta\chi^2_{i\,\rm max} = 6$, corresponding to the solid curve for π^-p and the dash-dotted curve for π^+p, reproduce the data reasonably well. On the other hand, the $\ln(\nu/m_\pi)$ fits are rather poor. Again the ρ data offer firm support for the Froissart bound fits, while ruling out $\ln(\nu/m_\pi)$ fits for the πp system.

Figure 4 shows an expanded scale of energies, in which *all* available πp cross sections are shown, from threshold to the highest available energies. The dashed curve is the *even* amplitude pion cross section $(\frac{\sigma_{\pi^+p}+\sigma_{\pi^-p}}{2})$ computed from our $\Delta\chi^2_{i\,\rm max} = 6$ cut, whereas the solid curve is the result of a similar analysis for the spin-averaged (even)

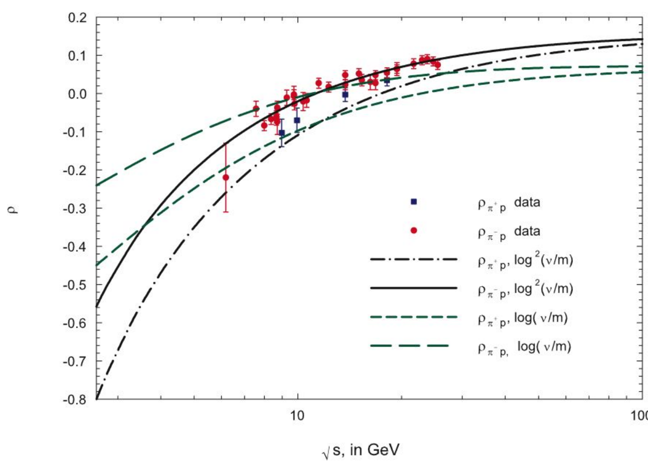

FIG. 3 (color online). The fitted ρ-values, ρ_{π^+p} and ρ_{π^-p}, *vs.* $\sqrt{s}$, in GeV, using the 4 constraints of Eqs. (12)–(15). The circles are the sieved data for π^-p scattering and the squares are the sieved data for π^+p scattering for $\sqrt{s} \ge 6$ GeV. The dash-dotted curve (π^+p) and the solid curve (π^-p) are χ^2 fits (Table II, $\sigma \sim \ln^2(\nu/m_\pi)$, $\Delta\chi^2_{i\,\rm max} = 6$) of the high energy data of the form: $\rho^\pm = \frac{1}{\sigma^\pm}\{\frac{\pi}{2}c_1 + c_2\pi\ln(\frac{\nu}{m}) - \beta_{\mathcal{P}'}\cot(\pi\mu/2)(\frac{\nu}{m})^{\mu-1} + \frac{4\pi}{\nu}f_+(0) \pm \delta\tan(\pi\alpha/2)(\frac{\nu}{m})^{\alpha-1}\}$. The upper sign is for π^+p and the lower sign is for π^-p scattering. The short dashed curve (π^+p) and the long dashed curve (π^-p) are χ^2 fits (Table II, $\sigma \sim \ln(\nu/m_\pi)$, $\Delta\chi^2_{i\,\rm max} = 6$) of the high energy data of the form: $\rho^\pm = \frac{1}{\sigma^\pm}\times\{\frac{\pi}{2}c_1 - \beta_{\mathcal{P}'}\cot(\pi\mu/2)(\frac{\nu}{m})^{\mu-1} + \frac{4\pi}{\nu}f_+(0) \pm \delta\tan(\pi\alpha/2)(\frac{\nu}{m})^{\alpha-1}\}$. The upper sign is for π^+p and the lower sign is for π^-p scattering. The laboratory energy of the pion is ν and m is the pion mass.

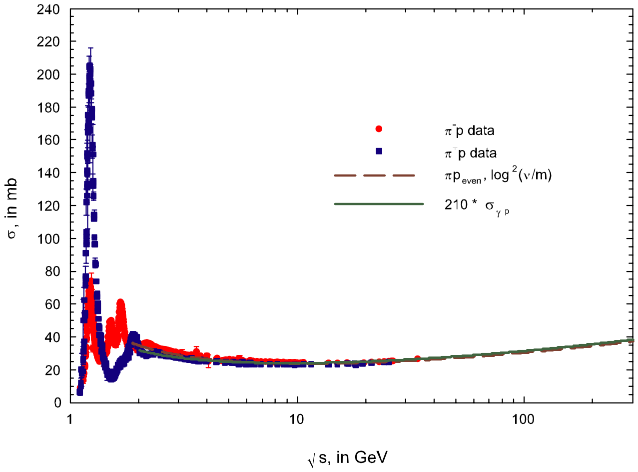

FIG. 4 (color online). The circles are the cross section data for $\pi^- p$ scattering and the squares are the cross section data for $\pi^+ p$ scattering, in mb, *vs.* $\sqrt{s}$, in GeV, for all of the known data. The dashed curve is the χ^2 fit (Table II, $\sigma \sim \ln^2(\nu/m_\pi)$, $\Delta\chi^2_{i\,\max} = 6$) to the high energy cross section data of the even amplitude cross section, of the form : $\sigma_{\pi p^{\rm even}} = c_0 + c_1 \ln(\frac{\nu}{m}) + c_2 \ln^2(\frac{\nu}{m}) + \beta_{\mathcal{P}'}(\frac{\nu}{m})^{\mu-1}$, with c_0 and $\beta_{\mathcal{P}'}$ constrained by Eq. (12) and (13). The laboratory energy of the pion is ν and m is the pion mass. The dashed curve is $210 \times \sigma_{\gamma p}$, from a fit of γp cross sections by Block and Halzen [5] of the form: $\sigma_{\gamma p} = c_0 + c_1 \ln(\nu/m_p) + c_2 \ln^2(\nu/m_p) + \beta_{\mathcal{P}'}/\sqrt{\nu/m_p}$, where m_p is the proton mass. The γp cross sections were fit for cms energies $\sqrt{s} \geq 2.01$ GeV, whereas the πp data (cross sections and ρ-values) were fit for cms energies $\sqrt{s} \geq 6$ GeV. The two fitted curves are virtually indistinguishable in the energy region $2 \leq \sqrt{s} \leq 300$ GeV.

cross section [5] for γp scattering, rescaled by multiplying it by 210, a familiar number from the vector dominance model. It is most striking that these two independent curves are virtually indistinguishable in the entire energy interval in which experimental data are available, *i.e.*, $2 \leq \sqrt{s} \leq 300$ GeV—a result most strongly supporting the vector dominance model.

All known πp cross section data are plotted in Fig. 5, which compares our analysis using the 4 constraint equations ($\Delta\chi^2_{i\,\max} = 6$ from Table II) with the analysis of Igi and Ishida [4] which used finite energy sum rules (FESR) for their low energy data. They only fitted the even cross section, so we have plotted in Fig. 5(a) the even portion of our $\ln^2(\nu/m_\pi)$ fit as the solid curve. It is seen to go smoothly through the *average* cross section, $(\frac{\sigma_{\pi^+ p} + \sigma_{\pi^- p}}{2})$, for pion-proton scattering. The dashed-dot curve, using the FESR, is from Igi and Ishida [4]. It does not go very smoothly through the average of the points, but rather goes much closer to $\sigma_{\pi^+ p}$ in the energy region from 10 to 30 GeV. Perhaps this is the result of their trying to fit *only* the even cross section, whereas we separately fit $\sigma_{\pi^+ p}$ and $\sigma_{\pi^- p}$. We have plotted in Fig. 5(b) the even portion of

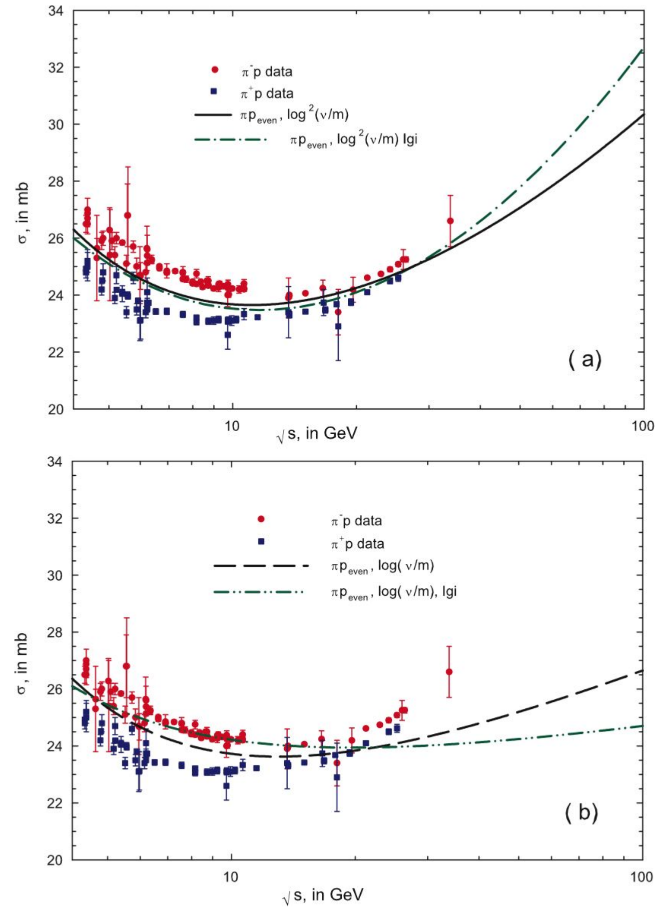

FIG. 5 (color online). The circles are the cross section data for $\pi^- p$ scattering and the squares are the cross section data for $\pi^+ p$ scattering for all known data, *vs.* $\sqrt{s}$, in GeV. The solid curve in (a) is the χ^2 fit (Table II, $\sigma \sim \ln^2(\nu/m_\pi)$, $\Delta\chi^2_{i\,\max} = 6$) to the high energy cross section data of the even amplitude, of the form : $\sigma_{\pi p^{\rm even}} = c_0 + c_1 \ln(\frac{\nu}{m}) + c_2 \ln^2(\frac{\nu}{m}) + \beta_{\mathcal{P}'}(\frac{\nu}{m})^{\mu-1}$, with c_0 and $\beta_{\mathcal{P}'}$ constrained by Eq. (12) and (13). The dash-dotted curve is an even amplitude $\ln^2(\nu/m_\pi)$ fit made by Igi and Ishida [4], using finite energy sum rules (FESR). The dashed curve in (b) is the χ^2 fit (Table II, $\sigma \sim \ln(\nu/m_\pi)$, $\Delta\chi^2_{i\,\max} = 6$) to the high energy cross section data of the even amplitude, of the form : $\sigma_{\pi p^{\rm even}} = c_0 + c_1 \ln(\frac{\nu}{m})) + \beta_{\mathcal{P}'}(\frac{\nu}{m})^{\mu-1}$, with c_0 and $\beta_{\mathcal{P}'}$ constrained by Eq. (12) and (13). The dot-dot-dashed curve is an even amplitude $\ln(\nu/m_\pi)$ fit made by Igi and Ishida [4], using finite energy sum rules. The laboratory energy of the pion is ν and m is the pion mass.

our $\ln(\nu/m_\pi)$ fit as the dashed curve, with the FESR result being the dashed-dot-dot curve. Clearly both curves rule out a $\ln(\nu/m_\pi)$ behavior. Both analyses strongly support a $\ln^2(\nu/m_\pi)$ behavior and thus a saturation of the Froissart bound for the πp system.

Figure 6 shows the individual fitted cross sections (in mb) for pp and $\bar{p}p$ for $\ln^2(\nu/m_p)$ and $\ln(\nu/m_p)$ for the cut $\Delta\chi^2_{i\,\max} = 6$ in Table III, plotted against the cms energy, $\sqrt{s}$, in GeV. The data shown are the sieved data with $\sqrt{s} \geq 6$ GeV. The $\ln^2(\nu/m_p)$ fits to the data sample with

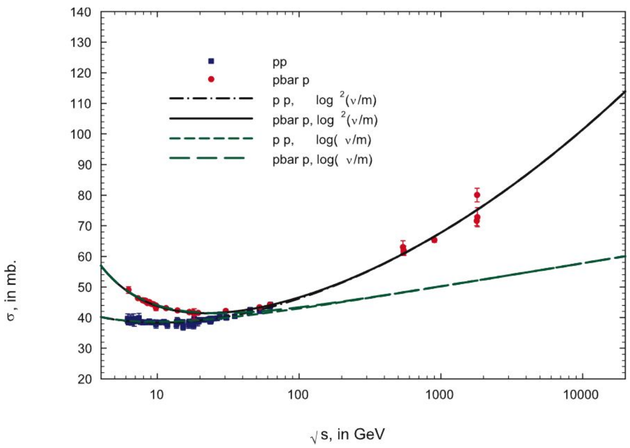

FIG. 6 (color online). The fitted total cross sections σ_{pp} and $\sigma_{\bar{p}p}$ in mb, *vs.* $\sqrt{s}$, in GeV, using the 4 constraints of Eqs. (12)–(15). The circles are the sieved data for $\bar{p}p$ scattering and the squares are the sieved data for pp scattering for $\sqrt{s} \geq 6$ GeV. The dash-dotted curve (pp) and the solid curve ($\bar{p}p$) are χ^2 fits (Table III, $\sigma \sim \ln^2(\nu/m_\pi)$, $\Delta\chi^2_{i\,\max} = 6$) of the high energy data of the form : $\sigma^{\pm} = c_0 + c_1 \ln(\frac{\nu}{m}) + c_2 \ln^2(\frac{\nu}{m}) + \beta_{\mathcal{P}'}(\frac{\nu}{m})^{\mu-1} \pm \delta(\frac{\nu}{m})^{\alpha-1}$. The upper sign is for pp and the lower sign is for $\bar{p}p$ scattering. The short dashed curve (pp) and the long dashed curve ($\bar{p}p$) are χ^2 fits (Table III, $\sigma \sim \ln(\nu/m_\pi)$, $\Delta\chi^2_{i\,\max} = 6$) of the high energy data of the form : $\sigma^{\pm} = c_0 + c_1 \ln(\frac{\nu}{m}) + \beta_{\mathcal{P}'}(\frac{\nu}{m})^{\mu-1} \pm \delta(\frac{\nu}{m})^{\alpha-1}$. The upper sign is for pp and the lower sign is for $\bar{p}p$ scattering. The laboratory energy of the nucleon is ν and m is the nucleon mass.

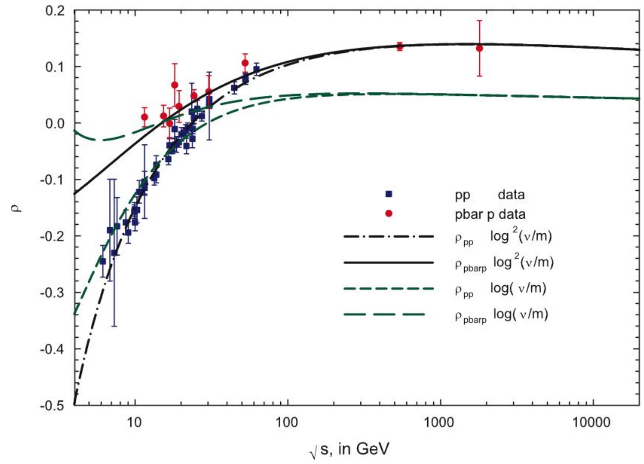

FIG. 7 (color online). The fitted ρ-values, ρ_{pp} and $\rho_{\bar{p}p}$, *vs.* $\sqrt{s}$, in GeV, using the 4 constraints of Eqs. (12)–(15). The circles are the sieved data for $\bar{p}p$ scattering and the squares are the sieved data for pp scattering for $\sqrt{s} \geq 6$ GeV. The dash-dotted curve (pp) and the solid curve ($\bar{p}p$) are χ^2 fits (Table III, $\sigma \sim \ln^2(\nu/m_\pi)$, $\Delta\chi^2_{i\,\max} = 6$) of the high energy data of the form : $\rho^{\pm} = \frac{1}{\sigma^{\pm}}\{\frac{\pi}{2}c_1 + c_2\pi\ln(\frac{\nu}{m}) - \beta_{\mathcal{P}'}\cot(\pi\mu/2)(\frac{\nu}{m})^{\mu-1} + \frac{4\pi}{\nu}f_+(0) \pm \delta\tan(\pi\alpha/2)(\frac{\nu}{m})^{\alpha-1}\}$. The upper sign is for pp and the lower sign is for $\bar{p}p$ scattering. The short dashed curve (pp) and the long dashed curve ($\bar{p}p$) are χ^2 fits (Table III, $\sigma \sim \ln(\nu/m_\pi)$, $\Delta\chi^2_{i\,\max} = 6$) of the high energy data of the form : $\rho^{\pm} = \frac{1}{\sigma^{\pm}} \times \{\frac{\pi}{2}c_1 - \beta_{\mathcal{P}'}\cot(\pi\mu/2)(\frac{\nu}{m})^{\mu-1} + \frac{4\pi}{\nu}f_+(0) \pm \delta\tan(\pi\alpha/2)(\frac{\nu}{m})^{\alpha-1}\}$. The upper sign is for pp and the lower sign is for $\bar{p}p$ scattering. The laboratory energy of the nucleon is ν and m is the nucleon mass.

$\Delta\chi^2_{i\,\max} = 6$, corresponding to the solid curve for $\bar{p}p$ and the dash-dotted curve for pp, are excellent, yielding a total renormalized $\chi^2 = 201.5$, for 184 degrees of freedom, corresponding to a fit probability of $\sim$0.2. On the other hand, the $\ln(\nu/m_p)$ fits to the same data sample—the long dashed curve for $\bar{p}p$ and the short dashed curve for pp—are very bad fits, yielding a total $\chi^2 = 2613.7$ for 185 degrees of freedom, corresponding to a fit probability of $<< 10^{-16}$. In essence, the $\ln(\nu/m_p)$ fit clearly undershoots *all* of the high energy cross sections. The ability of nucleon-nucleon scattering to distinguish cleanly between an energy dependence of $\ln^2(\nu/m_p)$ and an energy dependence of $\ln(\nu/m_p)$ is even more dramatic than the pion result.

Figure 7 shows the individual fitted ρ-values for pp and $\bar{p}p$ $\ln^2(\nu/m_p)$ and $\ln(\nu/m_p)$ from Table III, using $\Delta\chi^2_{i\,\max} = 6$—plotted against the cms energy, $\sqrt{s}$, in GeV. The data shown are the sieved data with $\sqrt{s} \geq 6$ GeV. The $\ln^2(\nu/m_p)$ fits, corresponding to the solid curve for $\bar{p}p$ and the dash-dotted curve for pp, fit the data reasonably well. On the other hand, the $\ln(\nu/m_p)$ fits, the long dashed curve for $\bar{p}p$ and the short dashed curve for pp, are very poor fits, missing completely the precise $\rho_{\bar{p}p}$ at 546 GeV, as well as $\rho_{\bar{p}p}$ at 1800 GeV. These results again strongly support the $\ln^2(\nu/m_p)$ fits that saturate the Froissart bound and once again rule out $\ln(\nu/m_p)$ fits for the $\bar{p}p$ and pp system.

A few remarks on our $\ln^2(\nu/m_p)$ asymptotic energy analysis for pp and $\bar{p}p$ are in order. It should be stressed that we used *both* the CDF and E710/E811 high energy experimental cross sections at $\sqrt{s} = 1800$ GeV in the $\ln^2(\nu/m_p)$ analysis, summarized in Table III, $\Delta\chi^2_{i\,\max} = 6$ and shown in Figs. 6 and 7. Inspection of Fig. 6 shows that at $\sqrt{s} = 1800$ GeV, our fit effectively passes below the cross section point of $\sim$80 mb (CDF collaboration). In particular, to test the sensitivity of our fit to the differences between the highest energy accelerator $\bar{p}p$ cross sections from the Tevatron, we next *omitted completely* the CDF ($\sim$ 80 mb) point and refitted the data without it. This fit, also using $\Delta\chi^2_{i\,\max} = 6$, had a renormalized χ^2/d.f. = 1.055, compared to 1.095 with the CDF point included. Since you only expect, on average, a $\Delta\chi^2$ of $\sim$1 for the removal of one point, the removal of the CDF point slightly improved the goodness-of-fit. Moreover, the new parameters of the fit were only *very minimally* changed. As an example, the predicted value from the new fit for the cross section at $\sqrt{s} = 1800$ GeV—*without* the CDF point—was $\sigma_{\bar{p}p} = 75.1 \pm 0.6$ mb, where the error is the statistical error due to the errors in the fitted parameters.

TABLE IV. Predictions of high energy $\bar{p}p$ and pp total cross sections and ρ-values, from Table III, $\sigma \sim \ln^2(\nu/m_\pi)$, $\Delta\chi^2_{i\,\mathrm{max}} = 6$.

$\sqrt{s}$, in GeV	$\sigma_{\bar{p}p}$, in mb	$\rho_{\bar{p}p}$	σ_{pp}, in mb	ρ_{pp}
6	48.97 ± 0.01	-0.087 ± 0.008	38.91 ± 0.01	$-.307 \pm 0.001$
60	43.86 ± 0.04	0.089 ± 0.001	43.20 ± 0.04	0.079 ± 0.001
100	46.59 ± 0.08	0.108 ± 0.001	46.23 ± 0.08	0.103 ± 0.001
300	55.03 ± 0.21	0.131 ± 0.001	54.93 ± 0.21	0.130 ± 0.002
400	57.76 ± 0.25	0.134 ± 0.002	57.68 ± 0.25	0.133 ± 0.002
540	60.81 ± 0.29	0.137 ± 0.002	60.76 ± 0.29	0.136 ± 0.002
1800	75.19 ± 0.55	0.139 ± 0.001	75.18 ± 0.55	0.139 ± 0.001
14 000	107.3 ± 1.2	0.132 ± 0.001	107.3 ± 1.2	0.132 ± 0.001
16 000	109.8 ± 1.3	0.131 ± 0.001	109.8 ± 1.3	0.131 ± 0.001
50 000	132.1 ± 1.7	0.124 ± 0.001	132.1 ± 1.7	0.124 ± 0.001
100 000	147.1 ± 2.0	0.120 ± 0.001	147.1 ± 2.0	0.120 ± 0.001

Conversely, the predicted value from Table IV—which used *both* the CDF and the E710/E811 point—was $\sigma_{\bar{p}p} = 75.2 \pm 0.6$ mb, virtually identical. Further, at $\sqrt{s} = 14$ TeV (LHC energy), the fit *without* the CDF point had $\sigma_{\bar{p}p} = 107.2 \pm 1.2$, whereas *including* the CDF point (Table IV) gave $\sigma_{\bar{p}p} = 107.3 \pm 1.2$. Thus, within errors, there was practically no effect of either including or excluding the CDF point. The fit was determined almost exclusively by the E710/E811 cross section—presumably because the asymptotic fit was locked into the low energy transition energy ν_0, thus sampling the rich amount of lower energy data.

Our result concerning the (un)importance of the CDF point relative to E710/E811 result is to be contrasted with the statement from the COMPETE Collaboration [3] which emphasized that there is: "the systematic uncertainty coming from the discrepancy between different FNAL measurements of σ_{tot}", which contribute large differences to their fit predictions at high energy, depending on which data set they use. In marked contrast to our results, they conclude that their fitting techniques favor the CDF point. Our results indicate that *both* the cross section and ρ-value of the E710/E811 groups are slightly favored. More importantly, we find virtually *no sensitivity* to high energy predictions when we do not use the CDF point and only use the E710/E811 measurements. Our method of fitting the data—by anchoring the asymptotic fit at the low transition energy ν_0—shows that our high energy predictions are quasi-independent of the FNAL "discrepancy", leading us to believe that our high energy cross section predictions at both the LHC and at cosmic ray energies are both robust and accurate. In Table IV, we give predictions—from our $\ln^2(\nu/m_p)$ fit—for some values of $\sigma_{\bar{p}p}$ and $\rho_{\bar{p}p}$ at high energies. The errors quoted are due to the statistical errors of the fitted parameters c_1, c_2 and $f_+(0)$ given in the $\Delta\chi^2_{i\,\mathrm{max}} = 6$, $\ln^2(\nu/m_p)$ fit of Table III.

In Fig. 8, we show an extended energy scale, from threshold up to cosmic ray energies ($1.876 \le \sqrt{s} \le 10^5$ GeV), plotting all available $\bar{p}p$ and pp cross sections, including cosmic ray pp cross sections inferred from cosmic ray p-air experiments by Block, Halzen and Stanev [11]. The solid curve is our result from Table III

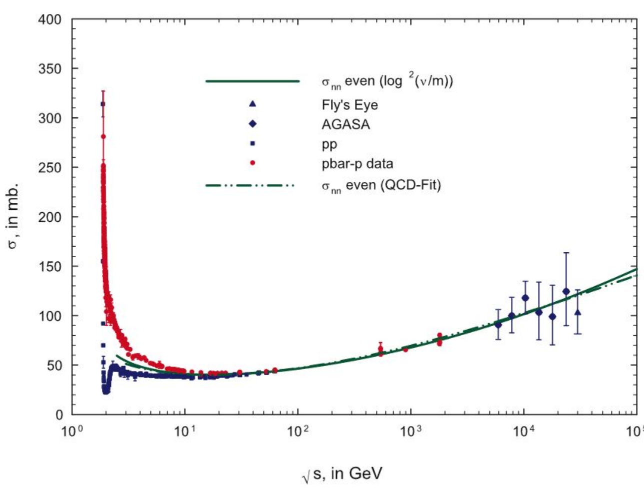

FIG. 8 (color online). The circles are the cross section data for $\bar{p}p$ scattering and the squares are the cross section data for pp scattering, in mb, *vs.* $\sqrt{s}$, in GeV, for all of the known accelerator data. The solid curve is the χ^2 fit (Table III, $\sigma \sim \ln^2(\nu/m_\pi)$, $\Delta\chi^2_{i\,\mathrm{max}} = 6$) of the high energy data of the crossing-even amplitude, of the form : $\sigma_{nn}\mathrm{even} = c_0 + c_1 \ln(\frac{\nu}{m}) + c_2 \ln^2(\frac{\nu}{m_p}) + \beta_{\mathcal{P}'}(\frac{\nu}{m})^{\mu-1}$, with c_0 and $\beta_{\mathcal{P}'}$ constrained by Eq. (12) and (13). The dot-dot-dashed curve is the crossing-even amplitude cross section σ_{nn}, from a QCD-inspired fit that fit not only the accelerator $\bar{p}p$ and pp cross sections and ρ-values, but also fit the AGASA and Fly's Eye cosmic ray pp cross sections shown in the figure—work done several years ago by Block, Halzen and Stanev (BHS group)[11]. The laboratory energy of the proton is ν and m is the proton mass. It is most striking that the two fitted curves for σ_{nn}even, using on the one hand, the $\ln^2(\nu/m)$ model of this work and on the other hand, the QCD-inspired model of the BHS group [11], are virtually indistinguishable over 5 decades of cms energy, *i.e.,* in the energy region $3 \le \sqrt{s} \le 10^5$ GeV.

of the *even* cross section from $\ln^2(\nu/m_p)$, $\Delta\chi^2_{i\,\max} = 6$. The dashed-dot-dot curve is from an independent QCD-inspired eikonal analysis [11] of the nucleon-nucleon system. The agreement is quite remarkable—the two independent curves are virtually indistinguishable over almost 5 decades of cms energy, from $\sim$3 GeV to 100 TeV. Figure 8 clearly indicates that the pp and $\bar{p}p$ cross section data greater than $\sim$3 GeV can be explained by a fit of the form $\sigma^{\pm} = c_0 + c_1 \ln(\frac{\nu}{m_p}) + c_2 \ln^2(\frac{\nu}{m_p}) + \beta_{\mathcal{P}'}(\frac{\nu}{m_p})^{\mu-1} \pm \delta(\frac{\nu}{m_p})^{\alpha-1}$ over an enormous energy range, i.e., by a $\ln^2 s$ saturation of the Froissart bound.

In Table IV, we make predictions of total cross sections and ρ-values for $\bar{p}p$ and pp scattering—in the low energy regions covered by RHIC, together with the energies of the Tevatron and LHC as well as the high energy regions appropriate to cosmic ray air shower experiments.

We give strong support to vector meson dominance by showing that the *even* cross section from our fits for $\pi^+ p$ and $\pi^- p$ data agrees exceedingly well with a $\sigma_{\gamma p}$ analysis (rescaled by the vector meson dominance factor taken to be 210 as in Ref. [5]) done earlier by Block and Halzen [5], when both cross sections have a $\ln^2 s$ asymptotic behavior.

In conclusion, we have demonstrated that the duality requirement that high energy cross sections smoothly interpolate into the resonance region strongly favors a $\ln^2 s$ behavior of the asymptotic cross sections for both the πp and nucleon-nucleon systems, in agreement with our earlier result for γp scattering [5]. We conclude that the three hadronic systems, γp, πp and nucleon-nucleon, *all* have an asymptotic $\ln^2 s$ behavior, thus saturating the Froissart bound.

At 14 TeV, we predict $\sigma_{\bar{p}p} = 107.3 \pm 1.1$ mb and $\rho_{\bar{p}p} = 0.132 \pm 0.001$ for the Large Hadron Collider—robust predictions that rely critically on the saturation of the Froissart bound.

The work of F. H. is supported in part by the U.S. Department of Energy under Grant No. DE-FG02-95ER40896 and in part by the University of Wisconsin Research Committee with funds granted by the Wisconsin Alumni Research Foundation.

[1] M. Froissart, Phys. Rev. **123**, 1053 (1961).
[2] M. M. Block, K. Kang, and A. R. White, Int. J. Mod. Phys. A **7**, 4449 (1992).
[3] J. R. Cudell *et al.*, Phys. Rev. D **65**, 074024 (2002); (COMPETE Collaboration), Phys. Rev. Lett. **89**, 201801 (2002).
[4] K. Igi and M. Ishida, Phys. Rev. D **66**, 034023 (2002) and references therein.
[5] M. M. Block and F. Halzen, hep-ph0405174; Phys. Rev. D **70**, 091901 (2004).
[6] M. M. Block and R. N. Cahn, Rev. Mod. Phys. **57**, 563 (1985).
[7] M. M. Block, Phys. Rev. D **65**, 116005 (2002).
[8] For the reaction $\gamma + p \rightarrow \gamma + p$, it is fixed as the Thompson scattering limit $f_+(0) = -\alpha/m = -3.03\mu$b GeV [see M. Damashek and F. J. Gilman, Phys. Rev. D **1**, 1319 (1970)].
[9] M. M. Block, physics/0506010.
[10] K. Hagiwara *et al.* (Particle Data Group), Phys. Rev. D **66**, 010001 (2002).
[11] M. M. Block, F. Halzen, and T. Stanev, Phys. Rev. Lett. **83**, 4926 (1999); Phys. Rev. D **62**, 077501 (2000).